2016

Axial-flexural interactions of GFRP-CFFT columns with and without reinforcing GFRP bars

Qasim S. Khan
University of Wollongong, qasim@uow.edu.au

M Neaz Sheikh
University of Wollongong, msheikh@uow.edu.au

Muhammad N. S Hadi
University of Wollongong, mhadi@uow.edu.au

Axial-flexural interactions of GFRP-CFFT columns with and without reinforcing GFRP bars

Abstract

This study presents the results of an experimental program and analytical modeling for axial-flexural interactions of concrete-filled glass fiber-reinforced polymer tube (GFRP-CFFT) columns with and without reinforcing glass fiber-reinforced polymer (GFRP) bars. The experimental program included four steel RC specimens, four GFRP-CFFT specimens, and four GFRP bar-reinforced GFRP-CFFT specimens with an outer diameter of 205-206 mm and a height of 800-812 mm. The specimens were tested under concentric and 25- and 50-mm eccentric axial loads and four-point load. The experimental results showed that GFRP bar-reinforced GFRP-CFFT specimens sustained higher peak axial loads, axial and lateral deformations at peak axial load, and flexural loads than GFRP-CFFT specimens without reinforcing GFRP bars and steel RC specimens. Axial load and bending moment (P-M) interactions of GFRP-CFFT specimens with and without reinforcing GFRP bars and steel RC specimens were analytically modeled. A parametric study was conducted to evaluate the effects of actual confinement ratio and GFRP bar reinforcement ratio on P-M interactions of GFRP-CFFT specimens. The P-M interactions were found to be significantly affected by both actual confinement ratio and GFRP bar reinforcement ratio.

Keywords

gfrp-cfft, axial-flexural, without, columns, gfrp, bars, interactions, reinforcing

Disciplines

Engineering | Science and Technology Studies

Publication Details

Khan, Q. S., Sheikh, M. Neaz. & Hadi, M. N. S. (2016). Axial-flexural interactions of GFRP-CFFT columns with and without reinforcing GFRP bars. Journal of Composites for Construction, Online First 1-12.

Axial-Flexural Interactions of Concrete Filled Glass Fiber Reinforced Polymer Tube (GFRP-CFFT) Columns with and without reinforcing GFRP bars

Qasim S. Khan[1], M. Neaz Sheikh[2] , Muhammad N.S. Hadi[3*] F.ASCE,

[1] Ph.D. Candidate, School of Civil, Mining and Environmental Engineering, University of Wollongong, Australia; formerly, Assistant Professor, Civil Engineering Department, University of Engineering and Technology, Lahore, Pakistan

[2] Senior Lecturer School of Civil, Mining and Environmental Engineering, University of Wollongong, Australia

[3*]Associate Professor, School of Civil, Mining and Environmental Engineering, University of Wollongong, Australia, Corresponding Author
Email: mhadi@uow.edu.au

Abstract

This study presents the results of an experimental program and analytical modelling for axial-flexural interactions of Concrete Filled Glass Fiber Reinforced Polymer Tube (GFRP-CFFT) columns with and without reinforcing Glass FRP (GFRP) bars. The experimental program included four steel Reinforced Concrete (RC) specimens, four GFRP-CFFT specimens and four GFRP bar reinforced GFRP-CFFT specimens of 205 – 206 mm outer diameter and 800 – 812 mm height. The specimens were tested under concentric, 25 mm and 50 mm eccentric axial loads and four-point load. The experimental results showed that GFRP bar reinforced GFRP-CFFT specimens sustained higher peak axial loads, axial and lateral deformations at peak axial load and flexural loads than GFRP-CFFT specimens without reinforcing GFRP bars and steel RC specimens. Axial load and bending moment ($P-M$) interactions of GFRP-CFFT specimens with and without reinforcing GFRP bars and steel RC specimens were analytically modelled. A parametric study was conducted to evaluate the effects of actual confinement ratio and GFRP bar reinforcement ratio on $P-M$ interactions of GFRP-

CFFT specimens. The $P-M$ interactions were found to be significantly affected by both actual confinement ratio and GFRP bar reinforcement ratio.

Keywords: GFRP-CFFT; GFRP bar; Axial loads; Four-point load; Stress-strain model; $P-M$ interaction

Introduction

Steel bar Reinforced Concrete (RC) columns are used in bridges and buildings to transfer loads from superstructure to substructure. The load carrying capacity of steel RC column reduces over the design life of the structure due to corrosion of steel bars. The large repair and maintenance costs and strength deterioration of steel RC columns over the design life are among the main concerns associated with steel RC columns. The National Association of Corrosion Engineers International reported that the United States annually spend about $2 billion for repairs and replacement of bridge piers and about $1 billion for marine piling systems (Mohamed *et al.* 2014). One of the solutions to reduce repair and maintenance costs is to use FRP reinforcement as a substitute of steel reinforcement for the construction of new concrete structures for increased service life and economy (Hadi *et al*. 2016a).

In the last two decades, Concrete Filled Fiber Reinforced Polymer Tube (CFFT) emerged as a new and attractive form of Fiber Reinforced Polymer (FRP) reinforcement for the construction of new structural members (e.g. bridge piers, building columns and overhead sign structures). In CFFT columns, FRP tube serves as lightweight formwork, barrier to corrosion accelerating agents, and longitudinal and transverse reinforcement (Mirmiran *et al.* 1998a; Lillistone and Jolly 2000). The FRP tube restrains the lateral dilation of confined concrete and thereby increases confined concrete strength and ultimate confined concrete strain of CFFT columns. Moreover, FRP tube was reported to be more efficient in increasing the confined concrete strength under axial and flexural loads than steel tubes (Fam and

Rizkalla 2001). The earlier studies demonstrated that CFFT columns sustained large inelastic deformations which makes FRP tube an attractive alternative of steel reinforcement for the construction of new concrete columns with high strength and ductility (Yamakawa *et al.* 2003; Gu *et al.* 2010). Several studies reported increased strength and ductility of CFFT columns under different load conditions due to higher effectiveness of FRP tube confinement than that of steel helix (Mirmiran *et al.* 1998b; Xiao *et al.* 1999; Fam and Rizkalla 2001, 2002; Hong and Kim 2004; Fam *et al.* 2005; Ozbakkaloglu and Saatcioglu 2006; Zhu *et al.* 2006; Mohamed and Masmoudi 2008a; Mohamed and Masmoudi 2010; Ozbakkaloglu 2013; Vincent and Ozbakkaloglu 2013; Idris and Ozbakkaloglu 2014, 2015; Khan *et al*. 2016; Wang *et al*. 2016).

In recent years, the use of FRP bar was investigated as a practicable alternative of steel bar in RC members for increased service life and reduced repair costs in harsh corrosive environments (Tobbi *et al.* 2012). FRP bars have excellent corrosion resistance and greater tensile strength to weight ratio than steel bar (Zadeh and Nanni 2013). The available studies on FRP bar reinforced concrete columns tested under concentric axial loads reported that FRP bar reinforced concrete columns resisted smaller axial loads than steel bar reinforced concrete column. De Luca *et al.* (2010) and Tobbi *et al.* (2012) reported that GFRP bar reinforced square concrete columns resisted 2.9 – 12% smaller axial loads than steel bar reinforced square concrete columns. Alsayed *et al.* (2012) reported that Glass FRP (GFRP) bar reinforced rectangular concrete columns resisted 13% smaller axial loads than steel bar reinforced rectangular concrete columns. Afifi *et al.* (2014a) reported that GFRP bar reinforced circular concrete columns resisted 7% smaller axial loads than steel bar reinforced circular concrete columns. Afifi *et al.* (2014b) reported that Carbon FRP (CFRP) bar reinforced circular concrete columns resisted 5% smaller axial loads than steel bar reinforced circular concrete columns. Hadi *et al.* (2016b) reported that GFRP bar reinforced circular

concrete columns resisted 12% smaller axial loads than steel bar reinforced circular concrete columns. However, FRP bar reinforced concrete columns exhibited significantly reduced corrosion than steel RC columns. Pantelides *et al.* (2013) reported that in hybrid (steel bars and GFRP helix) reinforced concrete columns minor level of corrosion was observed with no visible detrimental effect on the steel bars and in GFRP bar reinforced concrete columns almost no corrosion was observed.

A number of research studies investigated the application of FRP bars as longitudinal reinforcement in FRP bar reinforced concrete columns tested under axial load. However, ACI 440.1R (2006) does not recommend the use of FRP bars as longitudinal reinforcement in FRP bar reinforced concrete columns under axial load as FRP bars have lower ultimate strength in compression than in tension. The CSA S806 (2012) permits the use of FRP bars as longitudinal reinforcement in FRP bar reinforced concrete columns under axial load but ignores the contribution of FRP bars in ultimate axial load capacity. The ACI 440.1R-15 (ACI 2015) does not include any recommendation for the use of FRP bars as longitudinal reinforcement in FRP bar reinforced concrete columns.

In recent years, a small number of research studies investigated axial load and ductility of steel bar reinforced Concrete Filled Glass Fiber Reinforced Polymer Tube (GFRP-CFFT) columns under concentric and eccentric axial loads. Mohamed and Masmoudi (2008b) reported that steel bar reinforced GFRP-CFFT columns sustained larger axial loads and ductility than unreinforced GFRP-CFFT columns due to the dowel action of steel bars. Mohamed and Masmoudi (2008a) reported that peak axial loads of steel bar reinforced GFRP-CFFT columns were reduced by 48.3%, 61.1%, 70.8% and 77.0% under applied axial load eccentricity of 15, 30, 45 and 60 mm, respectively, compared to the peak axial loads of steel bar reinforced GFRP-CFFT columns under concentric axial load.

Most of the available research studies investigated the behavior of FRP bar reinforced concrete columns under concentric axial load. Although, columns in buildings are often subjected to combined axial load and bending moment due to construction errors, lateral loads and applied end moments (Hadi *et al.* 2013). To the knowledge of the authors, Fam *et al*. (2003) investigated the experimental and analytical axial load and bending moment interactions of high strength concrete filled GFRP tubes and Mohamed and Masmoudi (2008a) investigated the experimental axial load and bending moment interactions of steel bar reinforced normal strength concrete filled GFRP tubes. None of the studies investigated the experimental and analytical axial load and bending moment interactions of normal strength concrete filled GFRP tubes with and without reinforcing GFRP bars. This study investigates experimentally and analytically the axial load and bending moment interactions of Concrete Filled Glass Fiber Reinforced Polymer Tube (GFRP-CFFT) and GFRP bar reinforced GFRP-CFFT specimens.

Experimental Program

The details of the experimental program with adequate illustrations of the test set up and test specimens were presented in Hadi *et al*. (2016a). For clarity, the experimental program is briefly reviewed herein. The experimental program comprised four steel bar Reinforced Concrete (RC) specimens, four Concrete Filled Glass Fiber Reinforced Polymer Tube (GFRP-CFFT) specimens and four GFRP bar reinforced GFRP-CFFT specimens. All specimens were tested at the High Bay Laboratories, School of Civil, Mining and Environmental Engineering, University of Wollongong, Australia. The specimens were divided into three groups with four specimens in each group. The first group, REF consisted of steel RC specimens. The second group, GT consisted of GFRP-CFFT specimens. The third group, GTGR consisted of GFRP bar reinforced GFRP-CFFT specimens. From each group, the first specimen was tested under concentric axial load. The second specimen was tested

under 25 mm eccentric axial load. The third specimen was tested under 50 mm eccentric axial load. The fourth specimen was tested under four-point load. The specimens were labelled in two parts. The first part represents the type of specimen (REF, GT and GTGR). The second part represents the load condition (0 for concentric axial load, 25 and 50 for 25 mm and 50 mm eccentric axial loads, respectively and B for four-point load). The test matrix is presented in Table 1.

The REF group was reinforced longitudinally with six N12 (12 mm diameter deformed) steel bars and helically with R10 (10 mm diameter plain bar) steel helix of 155 mm diameter center to center with a pitch of 60 mm. In the REF group, a concrete clear cover of 15 mm at the top and bottom ends and a concrete clear cover of 20 mm at the side of the specimen were provided. The basis for the design of GT and GTGR groups was to devise alternatives of REF groups for regions where corrosion of steel reinforcement is a major concern. For GT and GTGR groups, GFRP tubes of 1.5 mm nominal thickness with inner layers of fibers oriented at 90° to the longitudinal direction and outer layers of fibers oriented at ±60° to the longitudinal direction were selected (CST Composites 2014). In GFRP tubes, 38% of the fibers were oriented along the circumferential direction and 62% of the fibers were oriented along the skew direction. The GFRP tubes consisted of 60% fibers and 40% resin by volume. The modulus of elasticity and ultimate tensile strength of GFRP tubes in the circumferential direction were 18 GPa and 810 MPa, respectively. The modulus of elasticity and ultimate tensile strength of GFRP tubes in the longitudinal direction were 5.4 GPa and 92.2 MPa, respectively (CST Composites). In GTGR group, six sand coated GFRP bars (15.9 mm nominal diameter) with all fibers oriented along the longitudinal direction (Pultruded bars) were glued to the inner side of GFRP tube (60° apart) along the circumference. The GTGR specimens were reinforced with 15.9 mm diameter GFRP bars and the REF specimens were reinforced with 12 mm diameter steel bars to have similar nominal axial load capacity. It is

noted that elastic modulus of GFRP bars was lower than steel bars. Thus, for the same diameter, the axial stiffness of GFRP bars was lower than that of steel bars. In GTGR group, a concrete clear cover of 15 mm at top and bottom ends was provided.

All groups were cast with ready mix concrete obtained from a local manufacturer. All groups were cured by covering them with wet hessian rugs and plastic sheets. The REF group was removed from the formworks after 7 days. All groups were cured for 28 days. The 28 days average compressive strength of concrete cylinders tested based on AS 1012.9-1999 (AS 1999) was 37 MPa. The measured cross-sectional area of GFRP bar was 292 mm^2 (19.3 mm diameter) based on immersion testing according to ISO 10461-1 (ISO 2015). The manufacturer provided nominal cross-sectional area of GFRP bar was 198 mm^2 (15.9 mm diameter) (V-Rod 2012). The difference in measured and nominal cross-sectional areas of GFRP bar was due to the sand coat to enhance bonding with surrounding concrete. The nominal cross-sectional area of GFRP bar was used to calculate ultimate strength and modulus of elasticity of GFRP bar in tension and compression in this study. The average tensile strength of GFRP bar was 1395 MPa and tensile modulus of elasticity of GFRP bar was 56 GPa measured according to ASTM D7205/D7205M-2011 (ASTM 2011). The average compressive strength of GFRP bar was 846 MPa and the average compressive modulus of elasticity of GFRP bar was 42 GPa measured according to ASTM D695-2010 (ASTM 2010). The nominal average tensile strengths of R10 and N12 bars were 400 MPa and 600 MPa, respectively, tested according to AS 1391-2007 (AS 2007).

Instrumentation and Test Procedures

The test groups were instrumented internally and externally to measure strains and deformations in the reinforcement. In REF group, two strain gauges were attached on steel helix at mid-height of the specimens (180° apart) to measure the circumferential strains in

steel helix and two strain gauges were attached on two steel bars at mid-height of the specimens (180° apart) to measure the axial strains in steel bars. For GT and GTGR groups, a pair of strain gauges was attached in the circumferential direction at mid-height of the specimens (180° apart) to measure the circumferential strains in GFRP tube. In addition, GTGR group was instrumented with two pairs of strain gauges fixed on two GFRP bars at mid-height of the specimens (180° apart) to measure the axial strains in GFRP bars. A laser triangulation was fixed at mid-height of the specimens tested under eccentric axial loads to measure the lateral deformations. Also, a laser triangulation was fixed at midspan of the specimens tested under four-point load to measure the midspan deflections. All groups were instrumented with two Linear Variable Displacement Transducers (LVDTs) fixed diagonally in the test machine (180° apart) to measure the axial deformations. All groups were tested in the 5000 kN Denison Universal Testing Machine (UTM). The specimens in all groups were preloaded to 100 kN and unloaded to 20 kN under a force controlled load application at a rate of 50 kN/min. Initial loading-unloading was carried out so that the specimen placed in the UTM is aligned properly to the loading plates. Afterwards, testing was resumed under a displacement controlled load application at a rate of 0.3 – 0.5 mm/min until the failure of the specimen.

Test Results and Discussion

Experimental results of specimens in all groups tested under different applied axial load eccentricity are presented in Table 2. The experimental results showed that increase in applied axial load eccentricity resulted in larger reduction in peak axial loads and corresponding axial deformations in GT and GTGR groups than in REF group, as GFRP reinforcement has smaller modulus of elasticity than steel reinforcement. The increase in applied axial load eccentricity resulted in larger increase in lateral deformations at peak axial load in GT and GTGR groups than in REF group. The circumferential strains in GFRP tube

at mid-height of specimens in GT and GTGR groups at peak axial loads were larger than the circumferential strains in steel helix at mid-height of REF group at peak axial loads under different applied axial load eccentricity. The larger measured circumferential strains in GT and GTGR groups were because GFRP tubes provided continuous confinement to the concrete. Also, two-thirds of the fibers in GFRP tube were oriented along the circumferential direction which was effective in restraining the lateral dilation of the confined concrete. The large difference between the mid-height circumferential strain at peak axial load of Specimens GT-0 and GTGR-0 was attributed to the different failure location of the specimens. Specimen GT-0 failed at the mid-height of specimen from rupturing of fibers and crushing of concrete. Specimen GTGR-0 failed in top one-third height of the specimen from rupturing of fibers, and crushing of concrete and rupturing of the top end of GFRP bars. Fanggi and Ozbakkaloglu (2015) also reported differences in the circumferential stresses and strains due to the different failure locations of CFFT specimens. The differences between the mid-height circumferential strains at peak axial load of Specimens GT-25 and GTGR-25, and Specimens GT-50 and GTGR-50 were small as the test specimens failed at the mid-height of the specimens from rupturing of fibers and crushing of concrete.

The GTGR group carried about 63% larger peak axial loads than GT group tested under different applied axial load eccentricity. This was attributed to the addition of GFRP bars in GTGR group which were effective in carrying axial loads. The measured axial strain in GFRP bars at peak axial load in GTGR group was about 72% of the measured axial strain in steel bars at peak axial load in REF group under different applied axial load eccentricity. The smaller axial strains in GFRP bars than steel bars are because of smaller modulus of elasticity of GFRP bar than steel bar. The experimental results showed that GFRP bars were effective in resisting axial loads and their contribution in ultimate axial load capacity should be properly accounted.

227 Experimental results of specimens in all groups tested under four-point load are presented in
228 Table 3. Specimen GT-B resisted 66.6% smaller peak flexural load than Specimen REF-B.
229 This was because only one-third of the fibers in GFRP tube were oriented along the
230 longitudinal direction which was effective in resisting flexural loads. Specimen GTGR-B
231 resisted 29.3% larger peak flexural load than Specimen REF-B. This was because of the
232 addition of GFRP bars in Specimen GTGR-B. Moreover, the measured strains in GFRP bars
233 in Specimen GTGR-B were about 40% of the measured strains in steel bars in Specimen
234 REF-B which showed that GFRP bars were effective in resisting flexural load. Specimens
235 GT-B and GTGR-B exhibited large midspan deflections at peak flexural load and failed at
236 midspan due to rupture of FRP tube. Similar observations were also reported in Idris and
237 Ozbakkaloglu (2014, 2015) for FRP concrete steel double skin tubular specimens.

238 During the test no slippage at the interface of GFRP tube and concrete under four-point load
239 (Specimens GT-B and GTGR-B) was observed. The bond between concrete and GFRP tube
240 at the ends of Specimens GT-B and GTGR-B was intact without any significant sign of
241 slippage. The measured tensile strain in the GFRP tube at midspan of Specimen GT-B and
242 Specimen GTGR-B were 4.3 and 3.2 times larger, respectively, than the tensile strain in the
243 steel helix at midspan of Specimen REF-B.

244 ***Experimental Axial Load Bending Moment Interactions***

245 Experimental axial load bending moment ($P - M$) interactions were constructed using peak
246 axial loads and bending moments at the peak axial loads of REF, GT and GTGR groups
247 tested under concentric axial load, 25 mm and 50 mm eccentric axial loads and four-point
248 load (Fig. 1). In REF group, the peak axial load represents the maximum axial load carried by
249 the gross cross-section (concrete cover and core) of the specimen before the spalling of
250 concrete cover. In GT and GTGR groups, the peak axial load represents the maximum axial

load carried by GFRP-CFFT before rupturing of GFRP tube. The bending moment (M) of REF, GT and GTGR groups were calculated by taking into account the primary moment (M_1) due to applied axial load eccentricity (e) and the secondary moment (M_2) due to lateral deformations (δ) at the peak axial load. Bending moment (M) of specimens tested under applied axial load eccentricity was calculated using Equation (1) and bending moment of specimens tested under four-point load was calculated using Equation (2).

$$M = P\,(e + \delta) \tag{1}$$

$$M = \frac{Pl}{6} \tag{2}$$

where e is the applied axial load eccentricity and l is the span length of flexural test arrangement.

The experimental $P - M$ interactions of GT and REF groups were presented in Fig. 1. Specimen GT-0 carried 23.2% larger axial load than Specimen REF-0. Specimen GT-25 carried 3.2% smaller axial load than Specimen REF-25 and Specimen GT-50 carried 12% smaller axial load than Specimen REF-50. Specimen GT-25 exhibited 5.6% larger bending moment than Specimen REF-25. Specimen GT-50 exhibited 13.3% smaller bending moment than Specimen REF-50. Specimen GT-B exhibited 48.9% smaller bending moment than Specimen REF-B. The larger reduction in the peak axial loads and bending moments at peak axial loads in GT group than REF group was attributed to lower modulus of elasticity of GFRP tube than steel. The experimental results showed that GT group can only serve as an alternative of REF group under concentric axial load where corrosion of steel is a concern.

The Fig.1 shows the larger axial loads and bending moments of GTGR group than REF group. Specimen GTGR-0 carried 83.9% larger axial load than Specimen REF-0. Specimen GTGR-25 carried 67.5% larger axial load than Specimen REF-25 and Specimen GTGR-50

carried 53.2% larger axial load than Specimen REF-50. Specimen GTGR-25 exhibited 127.5% larger bending moment than Specimen REF-25 and Specimen GTGR-50 exhibited 100.9% larger bending moment than Specimen REF-50. Specimen GTGR-B exhibited 94.8% larger bending moment than Specimen REF-B. The larger peak axial loads and bending moments of GTGR group than REF group was because of the greater confinement effectiveness of GFRP tube in confining the concrete than the steel helix which resulted in larger peak axial loads and corresponding lateral deformations and bending moments. Also, the diameter of GFRP bar was larger than the steel bar and GFRP bars were effective in carrying axial loads. The experimental results showed that GTGR group can serve as an alternative of REF group under concentric and eccentric axial loads and four-point load where corrosion of steel is a concern.

The Fig.1 shows the smaller axial loads and bending moments of GT group than GTGR group. The Specimen GT-0 carried 33% smaller axial load than Specimen GTGR-0. Specimen GT-25 carried 42.2% smaller axial load than Specimen GTGR-25 and Specimen GT-50 carried 42.5% smaller axial load than Specimen GTGR-50. Specimen GT-25 exhibited 53.6% smaller bending moment than Specimen GTGR-25 and Specimen GT-50 exhibited 56.9% smaller bending moment than Specimen GTGR-50. Specimen GT-B exhibited 73.8% smaller bending moment than Specimen GTGR-B. The larger peak axial loads and bending moments in GTGR group than REF group is attributed to the addition of GFRP bars in GTGR group.

Analytical Modeling

Confinement Mechanism of FRP Confined Concrete

In circular FRP confined concrete columns, the lateral nominal confinement pressure (f_l) provided by FRP confinement is assumed to be uniformly distributed around the

296 circumference of the confined concrete column (Fig. 2). The confinement mechanism of FRP
297 confined concrete is based on strain compatibility between FRP confinement and confined
298 concrete, and equilibrium of forces acting on FRP confined concrete. Increase in applied
299 axial load results in increase in axial strain and corresponding increase in lateral strain in
300 concrete (expansion of concrete) due to Poisson's effect. The FRP confinement is of passive
301 type and is activated due to expansion of concrete under increasing applied axial load. The
302 nominal confinement pressure (f_l) exerted by FRP confinement along the circumferential
303 direction increases with expansion of concrete until FRP confinement is exhausted. Based on
304 the assumption of strain compatibility, the circumferential strain in FRP confinement is equal
305 to the lateral strain in confined concrete (De Lorenzis and Tepfers 2003). The f_l exerted by
306 FRP confinement along circumferential direction is obtained based on equilibrium of forces
307 acting on FRP confined concrete (Equation 3):

$$f_l = \frac{2E_{FRP}t_{FRP}\varepsilon_{fu}}{D} \tag{3}$$

308 where E_{FRP} is modulus of elasticity of FRP confinement in the circumferential direction, t_{FRP}
309 is the thickness of FRP confinement, ε_{fu} is the ultimate tensile strain of fibers and D is the
310 diameter of FRP confined concrete. Replacing ε_{fu} with the experimentally obtained
311 circumferential rupture strain of fibers (ε_{rup}) in Eq. 3 yields actual confinement pressure
312 ($f_{l,a}$) exerted by the FRP confinement as given in Eq. 4.

$$f_{l,a} = \frac{2E_{FRP}t_{FRP}\varepsilon_{rup}}{D} \tag{4}$$

313 The $f_{l,a}$ exerted by the FRP confinement is lower than the f_l exerted by the FRP
314 confinement due to the fact that ε_{rup} is lower than the ε_f due to manufacturing
315 imperfections, construction errors and complex material behavior of FRP and confined

316 concrete (Khan *et al.* 2016). The available stress-strain models for FRP confined concrete
317 which defined the stress-strain and ultimate confined concrete conditions (confined concrete
318 strength and ultimate confined concrete strain) of FRP confined concrete in terms of $f_{l,a}$ are
319 more accurate than the stress-strain models which defined the stress-strain and ultimate
320 confined concrete conditions in terms of f_l (Ozbakkaloglu *et al*. 2012).

321 ***Modeling of Concrete Filled GFRP Tube***

322 Stress-strain models for FRP confined concrete in circular sections are broadly classified into
323 design oriented models and analysis oriented models (Ozbakkaloglu *et al*. 2012). The design
324 oriented models are simple closed form regression equations and are considered suitable for
325 simple analytical modelling of FRP confined concrete. The design oriented models in
326 Samaan *et al.* (1998) and Lam and Teng (2003) were considered suitable for the modelling of
327 confined concrete in concrete Filled GFRP tubes in GT and GTGR groups. This is because
328 Samaan *et al.* (1998) and Lam and Teng (2003) models take into account the effect of FRP
329 confinement on the initial portion of the stress-strain curve and account for the strain
330 hardening and strain softening behavior of FRP confined concrete. Also, the parameters in
331 Samaan *et al*. (1998) and Lam and Teng (2003) models were calibrated with large
332 experimental test databases. The ACI 440.2R-08 (ACI 2008) adopted Lam and Teng (2003)
333 model with minor modifications for FRP confined concrete under axial force or combined
334 axial and bending forces.

335 Samaan *et al.* (1998) stress-strain model for FRP confined concrete expresses axial stress of
336 FRP confined concrete (f_c) at a given axial strain (ε_c), as given in Equation (5).

$$f_c = \frac{(E_c - E_2)\varepsilon_c}{\left[1+\left(\frac{(E_c - E_2)\varepsilon_c}{f_o}\right)^n\right]^{1/n}} + E_2\varepsilon_c \tag{5}$$

where E_c is the slope of the first ascending axial stress-strain curve and is equivalent to the elastic modulus of concrete, E_2 is the slope of the second ascending axial stress-strain curve, f_o is the axial stress at the intercept of the second slope with the axial stress axis and n is a curve shape parameter which mainly controls the curvature of the transition point. The parameters of Samaan *et al.* (1998) stress-strain model were calibrated with experimental results of 30 GFRP-CFFT cylinders, as given in Equations (6 – 8):

where

$$E_2 = 245.61 f_{co}^{\ 0.2} + 1.3456 \frac{E_{FRP} t_{FRP}}{D} \tag{6}$$

$$f_o = 0.872 f_{co} + 0.371 f_{l,a} + 6.258 \tag{7}$$

$$n = 1.5 \tag{8}$$

Also, Samaan *et al.* (1998) proposed expressions to calculate FRP confined concrete strength (f'_{cc}) (Equation 9) as a function of actual confinement pressure at ultimate ($f_{l,a}$) (Equation 4) and unconfined concrete strength (f_{co}) and ultimate FRP confined concrete strain (ε_{cu}) (Equation 10) as a function of f'_{cc}, f_o and E_2.

$$f'_{cc} = f_{co} + 6 f_{l,a}^{\ 0.7} \tag{9}$$

$$\varepsilon_{cu} = \frac{f'_{cc} - f_o}{E_2} \tag{10}$$

The model of Lam and Teng (2003) represents the stress-strain behavior of FRP confined concrete with two curves i.e., parabolic first curve followed by linear-elastic second curve. The parabolic curve meets the linear-elastic curve at a transition strain (ε_t), as given in Equations (11 – 12).

$$f_c = E_c\varepsilon_c - \frac{(E_c - E_2)^2}{4f_o}\varepsilon_c{}^2,\ 0 \le \varepsilon_c \le \varepsilon_t \tag{11}$$

$$f_c = f_o + E_2\varepsilon_c,\ \varepsilon_t \le \varepsilon_c \le \varepsilon_{cu} \tag{12}$$

352 The parameters of Lam and Teng (2003) stress-strain model were calibrated with
353 experimental results of 76 FRP confined concrete cylinders, as given in Equations (13 – 15).

$$\varepsilon_t = \frac{2f_o}{E_c - E_2} \tag{13}$$

$$f_o = f_{co} \tag{14}$$

$$E_2 = \frac{f'_{cc} - f_o}{\varepsilon_{cu}} \tag{15}$$

354 Also, Lam and Teng (2003) proposed expressions to calculate the FRP confined concrete
355 strength (f'_{cc}) (Equation 16) as a function of $f_{l,a}$ (Equation 4) and f_{co} and ultimate FRP
356 confined concrete strain (ε_{cu}) (Equation 17) as a function of $f_{l,a}$, f_{co}, ε_{rup} and ε_{co}.

$$f'_{cc} = f_{co} + 3.3f_{l,a} \tag{16}$$

$$\varepsilon_{cu} = \left[1.75 + 12\left(\frac{f_{l,a}}{f_{co}}\right)\left(\frac{\varepsilon_{rup}}{\varepsilon_{co}}\right)^{0.45}\right]\varepsilon_{co} \tag{17}$$

357 ***Modeling of FRP Bar***

358 The axial stress-strain behavior of FRP bar is linear elastic till rupture (Kobayashi and
359 Fujisaki 1995; Deitz *et al.* 2003; ACI:440.1R 2006). The axial stress in GFRP bar (f_{Gi}) at a
360 given axial strain (ε_{Gi}) was calculated as a function of modulus of elasticity of GFRP bar in
361 compression (E_{Gi}), as given in Equation (18):

$$f_{Gi} = E_{Gi}\varepsilon_{Gi} \tag{18}$$

362 ***Modeling of Steel Reinforced Concrete***

363 The ACI 318M-2011 (ACI 2011) design guidelines for structural concrete ignores the
364 contribution of steel helix confinement in the ultimate axial load capacity of steel RC column.
365 In REF group, the confinement effect of steel helix at peak axial load was also ignored. This
366 is because the circumferential strains in steel helix at peak axial load are 15% of the yield
367 strain of steel bar (Mohamed *et al.* 2014). In REF group, the whole cross-section was
368 analytically modeled as unconfined concrete cross-section with continuous axial stress-axial
369 strain curve of concrete proposed by Popovics (1973), as given in Equations (19 - 20):

$$\frac{f_c}{f_{co}} = \frac{\varepsilon_c}{\varepsilon_{co}} \frac{n'}{n-1+\left(\frac{\varepsilon_c}{\varepsilon_{co}}\right)n'} \tag{19}$$

370 where

$$n' = \frac{E_c}{E_c - \frac{f_{co}}{\varepsilon_{co}}} \tag{20}$$

371 where f_{co} is unconfined concrete strength, ε_{co} is unconfined concrete strain corresponding to
372 f_{co} and n' is a coefficient. In this study, ε_{co} was calculated using the expression proposed by
373 Tasdemir *et al.* (1998), as given in Equation (21).

$$\varepsilon_{co} = \frac{-0.067 f_{co}^{\ 2} + 29.9 f_{co} + 1053}{10^6} \tag{21}$$

374 The modulus of elasticity of concrete (E_c) was calculated as a function of f_{co} as given in
375 ACI 318M-2011 (ACI 2011) (Equation 22):

$$E_c = 4730\sqrt{f_{co}} \tag{22}$$

376

377

Modeling of Steel Bar

The axial stress-axial strain behavior of steel bar was analytically modeled as elastic-perfectly plastic. The axial stress in steel bar (f_s) at a given axial strain (ε_s) was calculated as a function of modulus of elasticity of steel bar (E_s), as given in Equation (23):

$$f_s = E_s f_s \leq f_y \tag{23}$$

where f_y is yield strength of steel bar.

Analytical Axial Load Bending Moment Interactions

Analytical axial load bending moment ($P - M$) interactions of GT and GTGR groups were constructed using Samaan *et al.* (1998) and Lam and Teng (2003) stress-strain models for FRP confined concrete. Analytical $P - M$ interactions of Specimens REF were constructed using axial stress-axial strain curve of concrete proposed by Popovics (1973). The layer-by-layer numerical integration method was used to analyze circular specimen cross-sections.

The axial load capacity of GT and GTGR groups under concentric axial load was calculated using Equation (24), whereas the axial load capacity of REF group under concentric axial load was calculated using Equation (25).

$$P_n = 0.85 f'_{cc} (A_g - A_{GFRP}) + \alpha f_{fu} A_{GFRP} \tag{24}$$

$$P_n = 0.85 f_{co} (A_g - A_s) + f_y A_s \tag{25}$$

where A_g is the gross sectional area of concrete, A_{GFRP} is the area of GFRP bars, A_s is the area of steel bars, f_{fu} is the ultimate tensile strength of GFRP bar and α is the reduction factor to account for lower compressive strength than tensile strength of GFRP bar. The reduction factor (α) of 0.61 based on the experimental results of tension and compression

tests of GFRP bars was considered in the analytical modeling of GFRP bars. The axial loads and bending moments of GT, GTGR and REF groups under 25 mm and 50 mm eccentric axial loads and four-point load were calculated using the layer-by-layer numerical integration method.

Layer-by-layer Numerical Integration Method

In the layer-by-layer numerical integration method the circular specimen cross-section was assumed to consist of n layers of unit height (Fig. 3a). It was assumed that plane sections remain plane after bending, tensile strength of concrete is negligible, strain distribution within the circular cross-section of specimen is linear and full composite action between GFRP tube and confined concrete is developed.

In GT and GTGR groups, axial strain (ε_c) at mid-height of each layer was calculated in terms of ultimate FRP confined concrete strain (ε_{cu}) (Equation 26):

$$\varepsilon_c = \varepsilon_{cu} \frac{d_N - \left(n*1 - \frac{1}{2}\right)}{d_N} \tag{26}$$

where d_N is depth of neutral axis. In REF group, axial strain (ε_c) at mid-height of each layer was also calculated using Equation (26) by substituting ultimate FRP confined concrete strain (ε_{cu}) with concrete crushing strain of 0.003. In GT and GTGR groups, the axial stress (f_c) at mid-height of each layer corresponding to axial strain (ε_c) was calculated with Samaan *et al.* (1998) and Lam and Teng (2003) stress-strain models for FRP confined concrete for comparison purposes. In REF group, the axial stress (f_c) at mid-height of each layer corresponding to axial strain (ε_c) was calculated with axial stress-axial strain curve of concrete proposed by Popovics (1973). In GT and GTGR groups, the forces in concrete (F_{ci})

and GFRP tube (F_{ti}) at mid-height of each layer were calculated using Equations (27) and (28), respectively.

$$F_{ci} = f_c A_i \tag{27}$$

$$F_{ti} = E_{FRP}\varepsilon_c (A_o - A_i) \tag{28}$$

where A_o is the outer area of GFRP-CFFT, A_i is the area of a layer. In REF group, only F_{ci} (Equation 27) at mid-height of each layer was calculated. In GT, GTGR and REF groups, the moment (M_i) at mid-height of each layer was calculated using Equation (29).

$$M_i = (F_{ci} + F_{Ti}) * \left(\frac{D_o}{2} - \left(n*1 - \frac{1}{2} \right) \right) \tag{29}$$

The longitudinal bars in GTGR and REF groups were placed at a distance (d_i) from the extreme compressive fiber in four layers (i.e. d_1, d_2, d_3 and d_4) (Fig. 3b). The strain (ε_{Gi}) in each GFRP bar layer was calculated using Equation (30) and strain in each steel bar (ε_{si}) layer was calculated using Equation (31).

$$\varepsilon_{Gi} = \varepsilon_{cu} \frac{d_N - d_i}{d_N} \tag{30}$$

$$\varepsilon_{si} = 0.003 \frac{d_N - d_i}{d_N} \tag{31}$$

The stress (f_{Gi}) in each GFRP bar was calculated using Equation (32) and the stress (f_{si}) in each steel bar was calculated using Equation (33).

$$f_{Gi} = E_{Gi}\varepsilon_{Gi} \le f_{fu} \tag{32}$$

$$f_{si} = E_s \varepsilon_{si} \le f_y \tag{33}$$

The force (F_{Gi}) in each GFRP bar was calculated using Equation (34) and the force (F_{si}) in each steel bar was calculated using Equation (35).

$$F_{Gi} = f_{Gi} A_{GFRP} \tag{34}$$

$$F_{si} = f_{si} A_s \tag{35}$$

The moment produced by GFRP bars (M_{GFRP}) about the centroid of the circular GFRP-CFFT cross-section was calculated using Equation (36). The moment produced by steel bars (M_{STEEL}) about the centroid of the circular REF cross-section was calculated using Equation (37).

$$M_{GFRP} = \sum F_{Gi} \left(\frac{D_o}{2} - d_i\right) \tag{36}$$

$$M_{STEEL} = \sum F_{si} \left(\frac{D_o}{2} - d_i\right) \tag{37}$$

Comparison of Analytical and Experimental Axial Load Bending Moment Interactions

The analytical axial load bending moment interactions are compared with the experimental axial load bending moment interactions to validate the developed analytical model. The GT and GTGR groups were designed as alternatives of steel RC (REF group) for the regions where corrosion of steel is a major concern. The analytical axial load bending moment ($P-M$) interactions of GT and GTGR groups are presented in Fig. 4. For GT group, analytical $P-M$ interaction constructed with Samaan *et al.* (1998) model matched well with the corresponding experimental $P-M$ interaction at concentric and eccentric axial loads and four-point load (Fig. 4a). For Specimens GT-0, GT-25 and GT-50, analytical axial loads calculated with Samaan *et al.* (1998) model were 89.3%, 91.5% and 81.3%, respectively, of the experimental axial loads. For Specimens GT-25, GT-50 and GT-B, analytical bending moments calculated with Samaan *et al.* (1998) model were 103.4%, 96.9% and 115.9%, respectively, of the experimental bending moments. For GT group, analytical $P-M$ interaction constructed with Lam and Teng (2003) model underestimated the axial

448 loads and bending moments of the corresponding experimental $P-M$ interaction (Fig. 4a).
449 For Specimens GT-0, GT-25 and GT-50, analytical axial loads calculated with Lam and Teng
450 (1998) model were 89.1%, 92.8% and 83.5%, respectively, of the experimental axial loads.
451 For Specimens GT-25, GT-50 and GT-B, analytical bending moments calculated with Lam
452 and Teng (1998) model were 95%, 92.4% and 97.2%, respectively, of the experimental
453 bending moments. In general for GT group, analytical axial loads and bending moments
454 calculated with Samaan *et al.* (1998) and Lam and Teng (2003) models resulted in
455 conservative estimates. This conservative estimate was because analytical axial loads and
456 bending moments were calculated based on ultimate GFRP confined concrete strain in
457 compression with Samaan *et al*. (1998) and Lam and Teng (1998) models. Moreover in
458 eccentrically loaded FRP confined concrete specimens, the actual confined concrete strain
459 may exceed the analytically computed FRP confined concrete strain in the compression
460 regions.

461 For GTGR groups, analytical $P-M$ interaction constructed with Samaan *et al.* (1998)
462 model matched very well with the corresponding experimental $P-M$ interaction at
463 concentric and eccentric axial loads and four-point load (Fig. 4b). For Specimens GTGR-0,
464 GTGR-25 and GTGR-50, analytical axial loads calculated using Samaan *et al*. (1998) model
465 were 93.5%, 102.5% and 116.7%, respectively, of the experimental axial loads. For
466 Specimens GTGR-25, GTGR-50 and GTGR-B, analytical bending moments calculated with
467 Samaan *et al*. (1998) model were 88.2%, 98.8% and 92.1%, respectively, of the experimental
468 bending moments. For GTGR group, analytical $P-M$ interaction constructed with Lam and
469 Teng (2003) model underestimated the axial loads and bending moments of the
470 corresponding experimental $P-M$ interaction. For Specimens GTGR-0, GTGR-25 and
471 GTGR-50, analytical axial loads calculated with Lam and Teng (1998) model were 93.3%,
472 87.6% and 102.3%, respectively, of the experimental axial loads. For Specimens GTGR-25,

GTGR-50 and GTGR-B, analytical bending moments calculated with Lam and Teng (1998) model were 69.8%, 82.4% and 88%, respectively, of the experimental bending moments. For GTGR group, analytical axial loads and bending moments calculated with Lam and Teng (2003) model were more conservative than those calculated with Samaan *et al.* (1998) model. This was because ultimate GFRP confined concrete strain computed with Lam and Teng (2003) model was smaller than ultimate GFRP confined concrete strain computed with Samaan *et al.* (1998) model. The smaller ultimate strains in GFRP confined concrete resulted in smaller strains in GFRP bars because of an assumption of strain compatibility between GFRP bar and GFRP tube confined concrete. The smaller strains in GFRP bars resulted in smaller stresses and corresponding smaller forces and bending moments in GFRP bars. Hence, analytical axial loads and bending moments of GTGR group predicted with Lam and Teng (2003) model were more conservative than those calculated with Samaan *et al*. (1998) model.

For REF group, analytical $P-M$ interaction constructed with axial stress-axial strain curve of concrete proposed by Popovics (1973) matched very well with the corresponding experimental $P-M$ curve at concentric and eccentric axial loads and four-point load (Fig. 5). For Specimens REF-0, REF-25 and REF-50, analytical axial loads were 93%, 97% and 93%, respectively, of the experimental axial loads. Similarly, for Specimens REF-25, REF-50 and REF-B, analytical bending moments were 90%, 90% and 92%, respectively, of the experimental bending moments. The analytical results showed that REF specimen can be accurately modeled as unconfined concrete specimen and this approach is consistent with the approach adopted by ACI 318M-2011 (ACI 2011) for design purposes. Also, the layer-by-layer numerical integration method adopted in this study can be used to accurately predict the axial loads and bending moments of GT, GTGR and REF groups.

Parametric Study

A parametric study was conducted to study the effects of actual confinement ratio and GFRP bar reinforcement ratio on axial loads and bending moments of GFRP-CFFT reinforced with GFRP bars (GTGR group) tested under concentric and eccentric axial loads and four-point load. The parametric study considered GFRP-CFFT (206 mm outer diameter and 812 mm height) reinforced with six GFRP bars (15.9 mm nominal diameter i.e., $\rho = 2.35\%$). The GTGR group with four actual confinement ratios (i.e., 0.1, 0.2, 0.3 and 0.4) and GFRP bar reinforcement ratio ($\rho = 3.67\%$) were considered to study the effect of actual confinement ratio ($f_{l,a}/f_{co}$) on $P-M$ interactions. The $f_{l,a}/f_{co}$ values chosen in this parametric study were greater than the limiting actual confinement ratio ($f_{l,a}/f_{co} \geq 0.073$) required to ensure a non-descending second branch in the axial stress-strain performance (ACI 2008). The GTGR group reinforced with GFRP bars of four different nominal diameters (9.5 mm, 12.7 mm, 15.9 mm and 19.1 mm) resulted in four different GFRP bar reinforcement ratios (i.e. 1.32%, 2.35%, 3.67% and 5.29%) and actual confinement ratio ($f_{l,a}/f_{co} = 0.2$) were also considered to study the effect of increasing GFRP bar reinforcement ratio on $P-M$ interactions. Samaan *et al.* (1998) stress-strain model for FRP confined concrete was used to analytically model GFRP-CFFT and the layer-by-layer numerical integration method was used to analyze circular specimen cross-section. The $P-M$ interactions were constructed using normalized axial loads (P^*) (Equation 38) and normalized bending moments (M^*) (Equation 39).

$$P^* = \frac{P}{f_{co}A_g} \tag{38}$$

$$M^* = \frac{M}{f_{co}A_g D} \tag{39}$$

Fig. 6(a) demonstrated the increased normalized axial loads and bending moments of GTGR group with increase in actual confinement ratios from 0.1 to 0.4. Fig. 6(a) also demonstrated that increasing actual confinement ratio resulted in larger increase in axial loads under concentric and eccentric axial loads than in flexural loads and corresponding bending moments under four-point load. This was because two-thirds of the fibers in GFRP tube were oriented along the circumferential direction which were effective in confining the dilated concrete core and hence increased the axial loads. However, fibers oriented in circumferential direction were less effective under four-point load and only one-third of fibers oriented perpendicular to circumferential direction, which were effective under four-point load.

Fig. 6(b) demonstrated that increasing GFRP bar reinforcement ratio resulted in increase in normalized axial loads and bending moments (enlarged $P-M$ curves) of GTGR group. Figure 6(b) also demonstrated that increasing GFRP bar reinforcement ratio resulted in slightly larger increase in flexural loads and corresponding bending moments than peak axial loads. This was because GFRP bars under four-point load were effective in resisting load and, also, GFRP bars have higher ultimate strength in tension than in compression.

Conclusions

This study investigated experimentally and analytically the axial-flexural ($P-M$) interactions of steel RC (REF), GFRP-CFFT (GT) and GFRP bar reinforced GFRP-CFFT (GTGR) groups. A parametric study was also conducted to determine the effects of actual confinement ratio and GFRP bar reinforcement ratio on axial-flexural interactions. The following conclusions are drawn based on the experimental and analytical results:

The experimental $P-M$ interaction of GTGR group was larger than $P-M$ interactions of GT and REF group as GTGR group resisted higher axial and flexural loads, and lateral

deformations at peak axial loads than GT and REF groups. The confinement effectiveness of GFRP tube was reduced with the increase in applied axial load eccentricity.

For GT and GTGR groups, analytical axial loads and bending moments calculated using Samaan *et al*. (1998) and Lam and Teng (2003) stress-strain models underestimated the experimental axial loads and bending moments resulting in conservative estimates. Also, the layer-by-layer numerical integration method adopted here can be used to accurately compute the axial loads and bending moments of GT, GTGR and REF groups.

The parametric study results showed that increase in confinement ratio resulted in larger increase in peak axial loads than flexural loads and corresponding bending moments of GTGR group. Increase in GFRP bar reinforcement ratio resulted in slightly larger increase in flexural load and corresponding bending moments than peak axial loads of GTGR group.

Based on the experimental and analytical results presented in this study, GTGR group can serve as an alternative of REF group under concentric and eccentric axial loads and flexural load in structural applications for which corrosion of steel bar is a concern. However, GT group can serve as an alternative of REF group only under concentric axial load.

Acknowledgements

The authors thank the University of Wollongong, Australia for providing the funding and facilities to carry out the experimental work. The authors also acknowledge the technical assistance provided by Technical Officer Mr. Fernando Escribano. The first author thanks the University of Engineering and Technology, Lahore and Higher Education Commission (HEC) of Pakistan and the University of Wollongong, Australia for funding his PhD studies.

References

ACI (American Concrete Institute) (2006). "Guide for the Design and Construction of Structural Concrete Reinforced with FRP Bars." *ACI 440.1R-06,* Farmington Hills, MI 48331, USA.

ACI (American Concrete Institute) (2008). Guide for the Design and Construction of Externally Bonded FRP Systems for Strengthening Concrete Structures. *ACI 440.2R*-2008. United States.

ACI (American Concrete Institute). (2011). "Building Code Requirements for Structural Concrete and Commentary." *ACI 318M-11,* Farmington Hills, MI 48331, USA.

ACI (American Concrete Institute). (2015). "Guide for the Design and Construction of Structural Concrete Reinforced with FRP Bars." *ACI 440.1R-15,* Farmington Hills, MI 48331, USA.

Afifi, M., Mohamed, H. & Benmokrane, B. (2014a). "Axial capacity of circular concrete columns reinforced with GFRP bars and spirals." *Journal of Composites for Construction,* 04013017.

Afifi, M., Mohamed, H. & Benmokrane, B. (2014b). "Strength and axial behavior of circular concrete columns reinforced with CFRP Bars and Spirals." *Journal of Composites for Construction,* 04013035.

Alsayed, S., Al-Salloum, Y., Almussallam, T., El-Gamal, S. & Aqel, M. (2012). "Performance of glass fiber reinforced polymer bars under elevated temperatures." *Composites Part B: Engineering,* 43**,** 2265-2271.

AS (Australian Standard). (1999). "Methods of testing concrete, Method 9: Determination of the compressive strength of concrete specimens. *AS 1012.9-1999.* Sydney, NSW: Standards Australia.

AS (Australian Standard). (2007). "Metallic materials-Tensile testing at ambient temperature." *AS1391-2007,* Sydney, NSW.

ASTM (American Society for Testing and Materials). (2010). "Standard Test Method for Compressive Properties of Rigid Plastics." *D695-10,* 100 Barr Harbor Drive, PO Box C700, West Conshohocken, PA 19428-2959, USA.

ASTM (American Society for Testing and Materials). (2011). "Standard Test Method for Tensile Properties of Fiber Reinforced Polymer Matrix Composite Bars." *D7205/D7205M-11,* 100 Barr Harbor Drive, PO Box C700, West Conshohocken, PA 19428-2959, USA.

CSA (Canadian Standards Association). (2012). "Design and construction of building components with fiber reinforced polymers." *CSA S806-12.* Toronto.

CST Composites 2014, accessed 30 March 2014, < http://www.cstcomposites.com/products-and-services/tubes-rods-and-components>

De Lorenzis, L. & Tepfers, R. (2003). "Comparative study of models on confinement of concrete cylinders with Fiber-Reinforced Polymer composites. *Journal of Composites for Construction,* 7**,** 219-237.

De Luca, A., Matta, F. & Nanni, A. (2010). "Behavior of full scale glass Fiber Reinforced Polymer reinforced concrete columns under axial load." *ACI Structural Journal,* 107**,** 589-596.

Deitz, D., Harik, I. & Gesund, H. (2003). "Physical properties of glass Fiber Reinforced Polymer rebars in compression." *Journal of Composites for Construction,* 7**,** 363-366.

610 Fam, A. & Rizkalla, S. (2001). "Concrete filled FRP tubes for flexural and axial compression
611 members." *ACMBS-MCAPC.*
612 Fam, A. & Rizkalla, S. (2002). "Flexural behavior of Concrete-Filled Fiber-Reinforced
613 Polymer circular tubes. *Journal of Composites for Construction,* 6**,** 123-132.
614 Fam, A., Flisak, B. & Rizkalla, S. (2003). "Experimental and analytical modelling of concrete
615 filled fiber reinforced polymer tubes subjected to combined bending and axial loads."
616 ACI Structural Journal, 100(4), 499-509.
617 Fam, A., Schnerch, D. & Rizkalla, S. (2005). "Rectangular Filament-Wound Glass Fiber
618 Reinforced Polymer Tubes Filled with Concrete under Flexural and Axial Loading:
619 Experimental Investigation. *Journal of Composites for Construction,* 9**,** 25-33.

620 Fanggi, B. A. L., and Ozbakkaloglu, T. (2015). "Behavior of hollow and concrete-filled FRP-
621 HSC and FRP-HSC-steel composite columns subjected to concentric compression."
622 Advances in Structural Engineering, 18(5), 715-738.

623 Gu, D., Wu, G., Wu, Z. & Wu, Y. (2010). "Confinement effectiveness of FRP in retrofitting
624 circular concrete columns under simulated seismic load." *Journal of Composites for*
625 *Construction,* 14**,** 531-540.

626 Hadi, M. N. S., Khan, Q. S. & Sheikh, M. N. (2016a). "Axial and flexural behavior of
627 unreinforced and FRP bar reinforced circular concrete filled FRP tube columns."
628 Construction and Building Materials, 122, 43-53.

629 Hadi, M. N. S., Karim H., & Sheikh M.N. (2016b). "Experimental investigations on circular
630 concrete columns reinforced with GFRP bars and helices under different loading
631 conditions". Journal of Composites for Construction;. (DOI: Permalink:
632 http://dx.doi.org/10.1061/(ASCE)CC.1943-5614.0000670)
633 Hadi, M. N. S., Pham, T. & Lei, X. (2013). "New method of strengthening reinforced
634 concrete square columns by circularizing and wrapping with Fiber-Reinforced
635 Polymer or steel straps. *Journal of Composites for Construction,* 17**,** 229-238.
636
637 Hong, W. K. & Kim, H. C. (2004). "Behavior of concrete columns confined by carbon
638 composites tubes." *Canadian Journal of Civil Engineering***,** 31(2), 178-188.

639 Idris, Y., & Ozbakkaloglu, T. (2014). "Flexural behavior of FRP-HSC steel composite
640 beams." Thin-Walled Structures, 80, 207-216.

641 Idris, Y., & Ozbakkaloglu, T. (2015). "Flexural behavior of FRP-HSC-steel double skin
642 tubular beams under reversed-cyclic loading." Thin-Walled Structures, 87, 89-101.

643 ISO (International Standard). (2015). "Fibre-reinforced polymer (FRP) reinforcement of
644 concrete - Test methods - Part 1: FRP bars and grids" *ISO 10406-1:2015*, Switzerland.

645 Khan, Q. S., Sheikh, M. N. & Hadi, M. N. S. (2016). "Axial compressive behavior of circular
646 CFFT: Experimental database and design oriented model." Steel and Composite
647 Structures, 21(4), 921-947.

648 Kobayashi, K. & Fujisaki, T. (1995). "Compressive behavior of FRP reinforcement in non-
649 prestressed concrete members." In Proc., The Second International RILEM

650 Symposium of Nonmetallic (FRP) reinforcement for concrete structures (FRPRCS-2),
651 London, England.
652 Lam, L. & Teng, J. G. (2003). "Design-oriented stress–strain model for FRP-confined
653 concrete." *Construction and Building Materials,* 17**,** 471-489.
654 Lillistone, D. & Jolly, C. K. (2000). "An innovative form of reinforcement for concrete
655 columns using advanced composites." *The Structural Engineer,* 78**,** 20-29.
656 Mirmiran, A., Samaan, M., Cabrera, S. & Shahawy, M. (1998a). "Design, manufacture and
657 testing of a new hybrid column." *Construction and Building Materials,* 12**,** 39-49.
658 Mirmiran, A., Shahawy, M. & Samaan, M. (1998b). "Strength and ductility of hybrid FRP-
659 Concrete beam-columns." *Journal of Structural Engineering,* 125**,** 1085-1093.
660 Mohamed, H. & Masmoudi, R. (2008a). "Behavior of the concrete filled FRP tube columns
661 under eccentric load." *Structural composites for Infrastructure Applications (MESC-*
662 *5).* Hurghada, Egypt.
663 Mohamed, H. & Masmoudi, R. (2008b). "Compressive behavior of reinforced concrete filled
664 FRP tubes." *ACI-SP,* SP-257**,** 91-108.
665 Mohamed, H. M. & Masmoudi, R. (2010). "Flexural strength and behavior of steel and FRP-
666 reinforced concrete-filled FRP tube beams." *Engineering Structures,* 32**,** 3789-3800.
667 Mohamed, M. H., Afifi, M. Z. & Benmokrane, B. (2014). "Performance evaluation of
668 concrete columns reinforced longitudinally with FRP Bars and confined with FRP
669 hoops and spirals under axial load." *Journal of Bridge Engineering,* 19**,** 04014020.
670 Ozbakkaloglu, T. & Saatcioglu, M. (2006). "Seismic behavior of high-strength concrete
671 columns confined by Fiber-Reinforced Polymer tubes." *Journal of Composites for*
672 *Construction,* 10**,** 538-549.
673 Ozbakkaloglu, T. (2013). "Compressive behavior of concrete-filled FRP tube columns:
674 Assessment of critical column parameters." *Engineering Structures,* 51**,** 188-199.
675 Pantelides, C., Gibbons, M. & Reaveley, L. (2013). "Axial load behavior of concrete columns
676 confined with GFRP spirals." *Journal of Composites for Construction,* 17**,** 305-313.
677 Popovics, S. (1973). "A numerical approach to the complete stress strain curves for
678 concrete." *Cement and Concrete Research,* 3**,** 583-599.
679 Samaan, M., Mirmiran, A. & Shahawy, M. (1998). Model of Concrete Confined by Fiber
680 Composites. *Journal of Structural Engineering,* 124**,** 1025-1031.
681 Tasdemir, M. A., Tasdemir, C., Akyüz, S., Jefferson, A. D., Lydon, F. D. & Barr, B. I. G.
682 (1998). "Evaluation of strains at peak stresses in concrete: A three-phase composite
683 model approach." *Cement and Concrete Composites,* 20**,** 301-318.
684 Tobbi, H., Farghaly, A. S. & Benmokrane, B. (2012). "Concrete columns reinforced
685 longitudinally and transversally with glass Fiber-Reinforced Polymer bars." *ACI*
686 *Structural Journal,* 109**,** 551-558.
687 Vincent, T. & Ozbakkaloglu, T. (2013). "Influence of fiber orientation and specimen end
688 condition on axial compressive behavior of FRP confined concrete." *Construction and*
689 *Building Materials,* 47**,** 814-826.
690 V-Rod (2012). "Composite reinforcing rods technical data sheet." Largs Bay SA, Australia.
691 Wang, W., Sheikh, M. N. & Hadi, M. N. S. (2016). “Experimental study on FRP tube
692 reinforced concrete columns under different loading conditions.” Journal of

693 Composites for Construction, http://dx.doi.org/10.1061/(ASCE)CC.1943-
694 5614.0000690.
695 Xiao, Y., Wu, H. & Martin, G. R. (1999). "Prefabricated composite jacketing of RC columns
696 for enhanced shear strength." *Journal of Structural Engineering,* 125**,** 255-264.
697 Yamakawa, T., Zhong, P. & Ohama, A. (2003). "Seismic performance of aramid fiber square
698 tubed concrete columns with metallic and/or non-metallic reinforcement." *Journal of*
699 *Reinforced Plastics and Composites,* 22**,** 1221-1238.
700 Zadeh, H. & Nanni, A. (2013). Design of RC columns using Glass FRP reinforcement."
701 *Journal of Composites for Construction,* 17**,** 294-304.
702 Zhu, Z., Ahmad, I. & Mirmiran, A. (2006). "Seismic performance of concrete-Filled FRP
703 tube columns for bridge substructure." *Journal of Bridge Engineering,* 11**,** 359-370.
704
705
706
707
708
709
710
711
712
713
714
715
716
717
718
719

720 **List of Tables**

724

725

726

727

728

729

730

731

732

733

734

735

736

737

738

739

740

741

742

List of Figures

760 **Table 1.** Experimental Program

Specimen ID	Outer diameter (mm)	Height (mm)	Lateral confinement	Longitudinal bars	Test Eccentricity
REF-0	205	800	Steel helix	Steel	0
REF-25	205	800	Steel helix	Steel	25
REF-50	205	800	Steel helix	Steel	50
REF-B	205	800	Steel helix	Steel	Four-point load
GT-0	206	812	GFRP tube	-	0
GT-25	206	812	GFRP tube	-	25
GT-50	206	812	GFRP tube	-	50
GT-B	206	812	GFRP tube	-	Four-point load
GTGR-0	206	812	GFRP tube	GFRP	0
GTGR-25	206	812	GFRP tube	GFRP	25
GTGR-50	206	812	GFRP tube	GFRP	50
GTGR-B	206	812	GFRP tube	GFRP	Four-point load

761

762

763 **Table 2.** Test results of column specimens

Specimen ID	Peak axial load (kN)	Axial deformation at peak axial load (mm)	Lateral deformation at peak axial load δ (mm)	Bending moment M (kN.m)	Mid-height circumferential strain on tension side at Peak axial load	Strain in bars at mid-height at peak axial load
REF-0	1529	2.4	-	-	0.0010	0.0156
REF-25	888	4.2	3.3	25.1	0.0005	0.0112
REF-50	594	3.2	3.2	31.6	0.0001	0.0075
GT-0	1884	21.3	-	-	0.0126	-
GT-25	860	4.2	5.8	26.5	0.0030	-
GT-50	523	4.1	4.0	28.2	0.0005	-
GTGR-0	2812	23.1	-	-	0.0032	0.0068
GTGR-25	1487	13.5	13.4	57.1	0.0077	0.0086
GTGR-50	910	11.6	21.0	64.6	0.0018	0.0072

764
765
766
767
768
769
770
771
772
773
774
775
776
777
778
779

780 **Table 3.** Test results of beam specimens

Specimen ID	Peak flexural load (kN)	Midspan deflection at peak flexural load (mm)	Bending Moment *M* (kN.m)	Longitudinal strain at midspan of specimen on tension side at Peak flexural load	Strain in bars at mid-height at peak flexural load	
					Compression side	Tension side
REF-B	347	37.3	27.0	0.0013	0.0237	0.0148
GT-B	116	27.1	13.8	0.0134	-	-
GTGR-B	448	27.1	52.7	0.0229	0.0068	0.0059

781

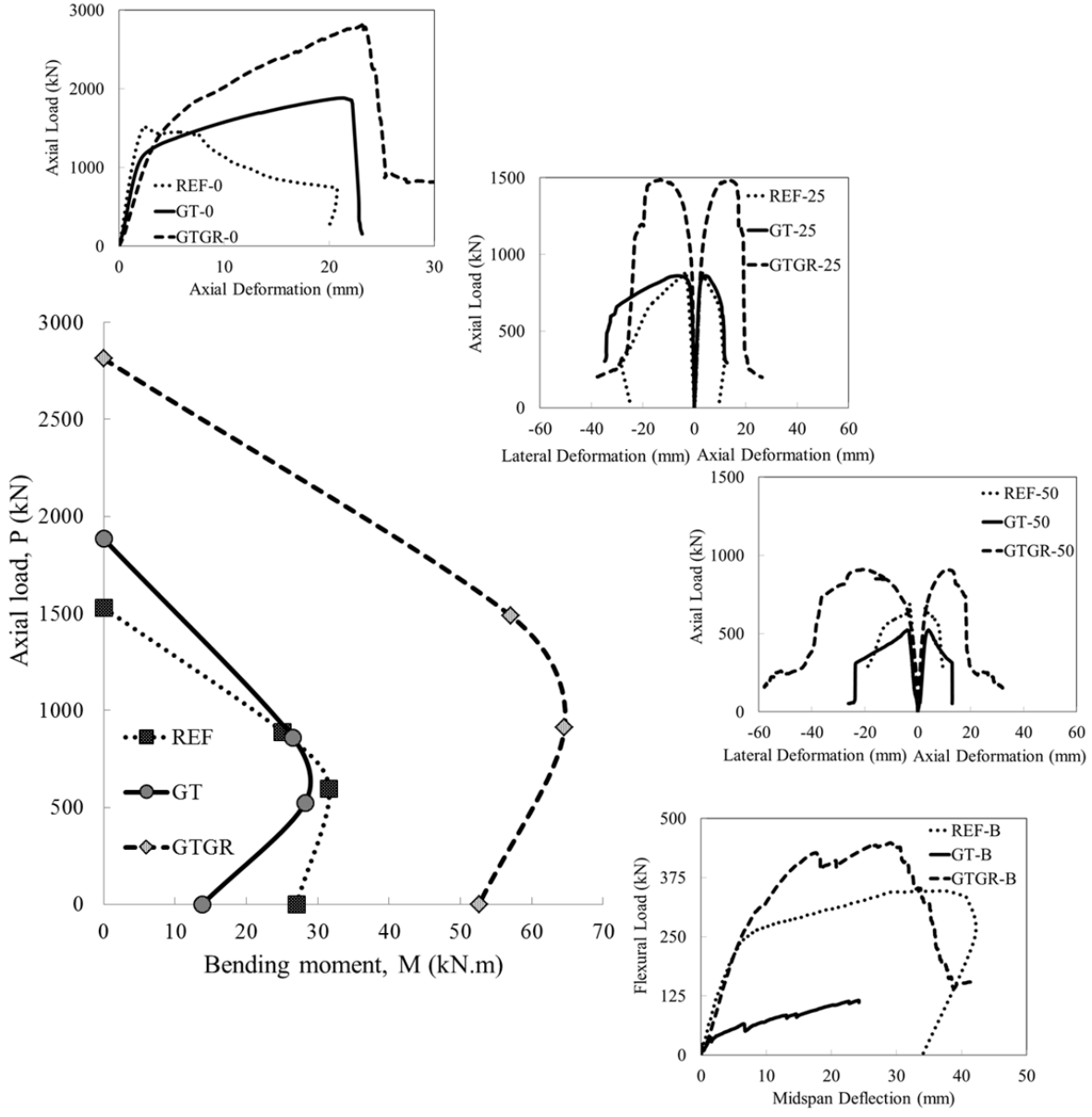

782
783

Fig. 1. Experimental axial load bending moment interactions of REF, GT and GTGR groups

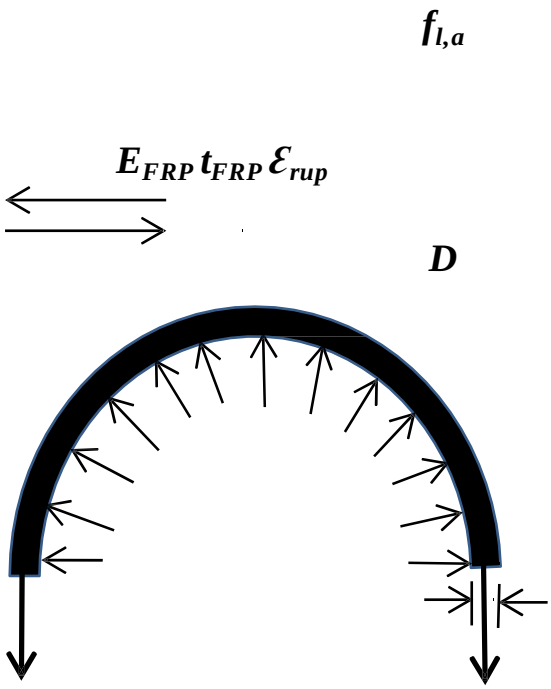

Fig. 2. Confinement mechanism of FRP confined concrete

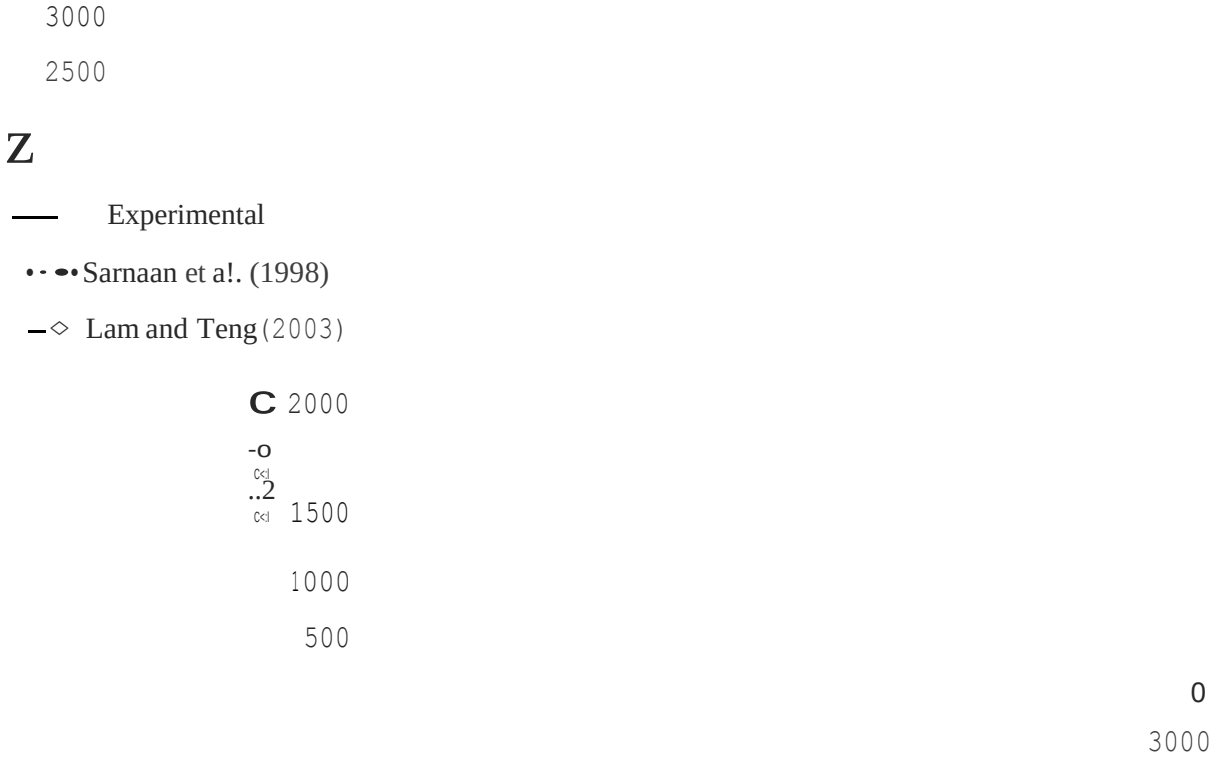

826
827
828
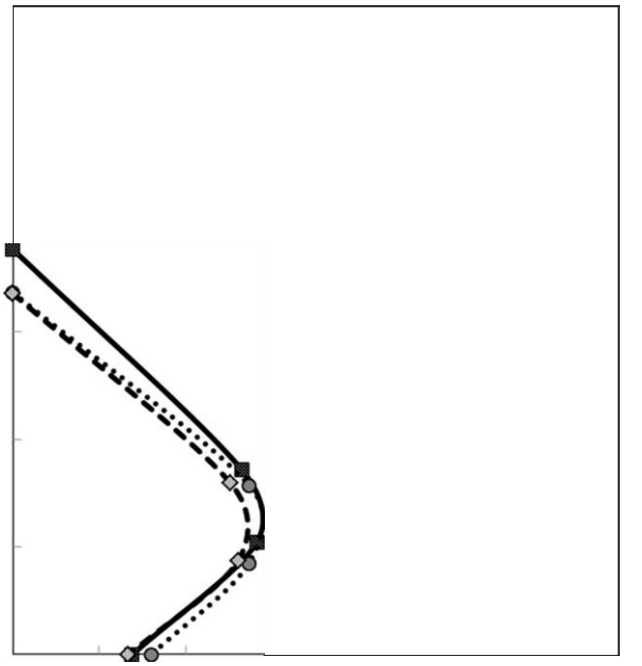

829
830 (a) GT
831

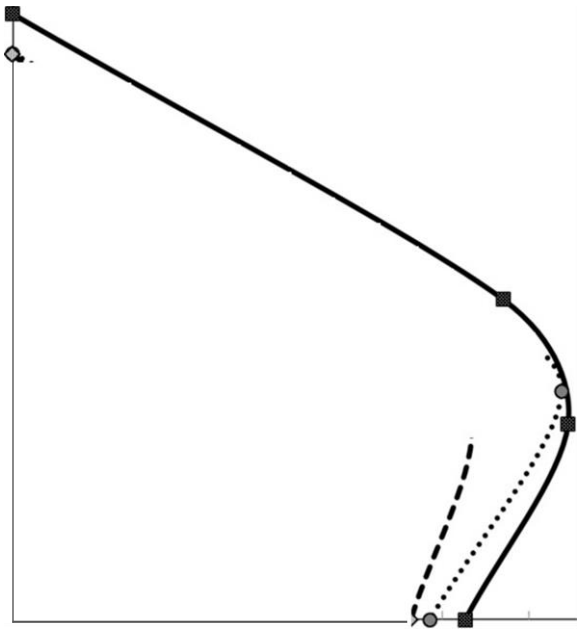

Experimental

2500

Samaan et a!. (1998)

Lam and Teng (2003)

2000

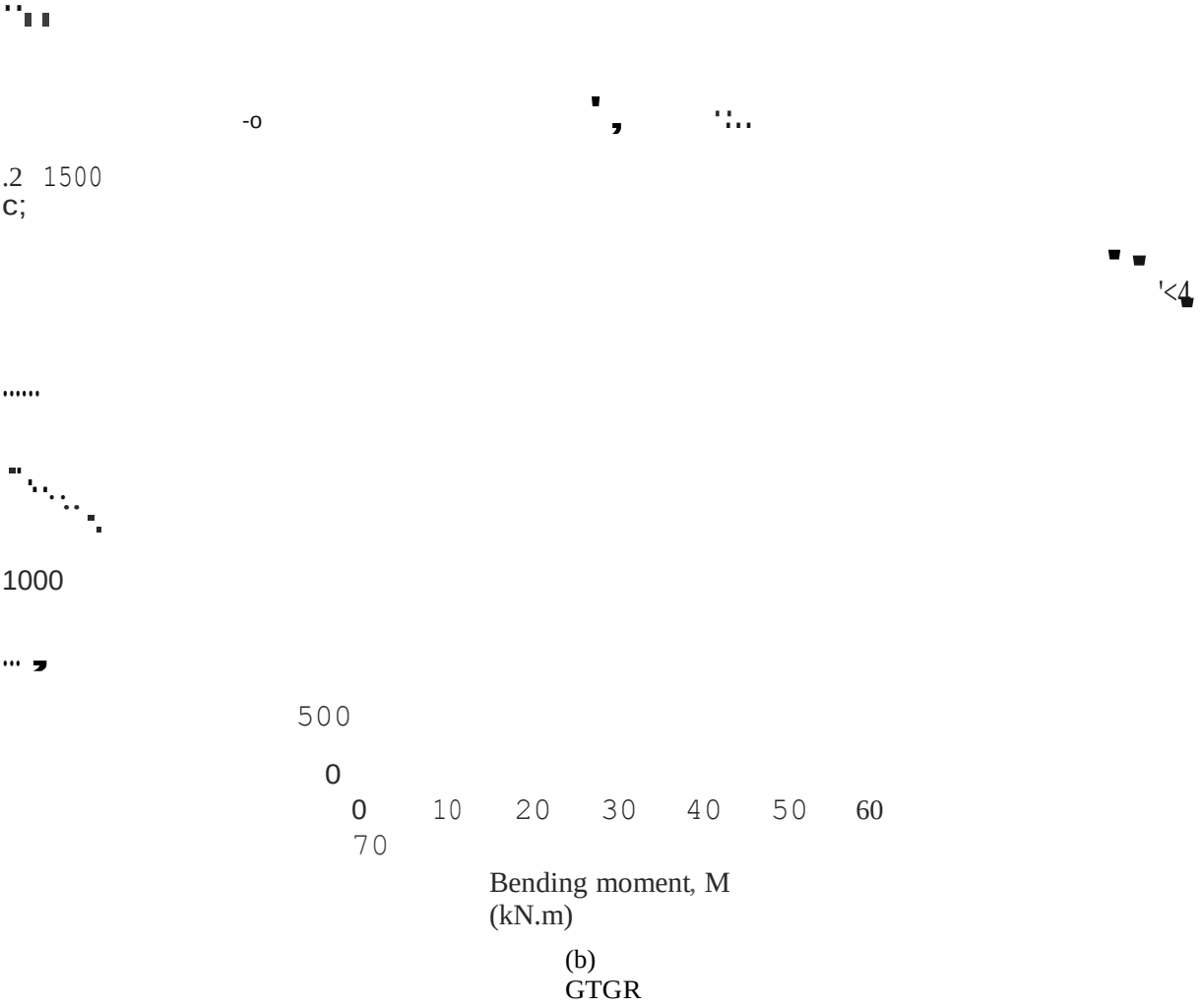

Fig. 4. Experimental and analytical axial load bending moment interactions of groups: (a) GT, and (b) GTGR

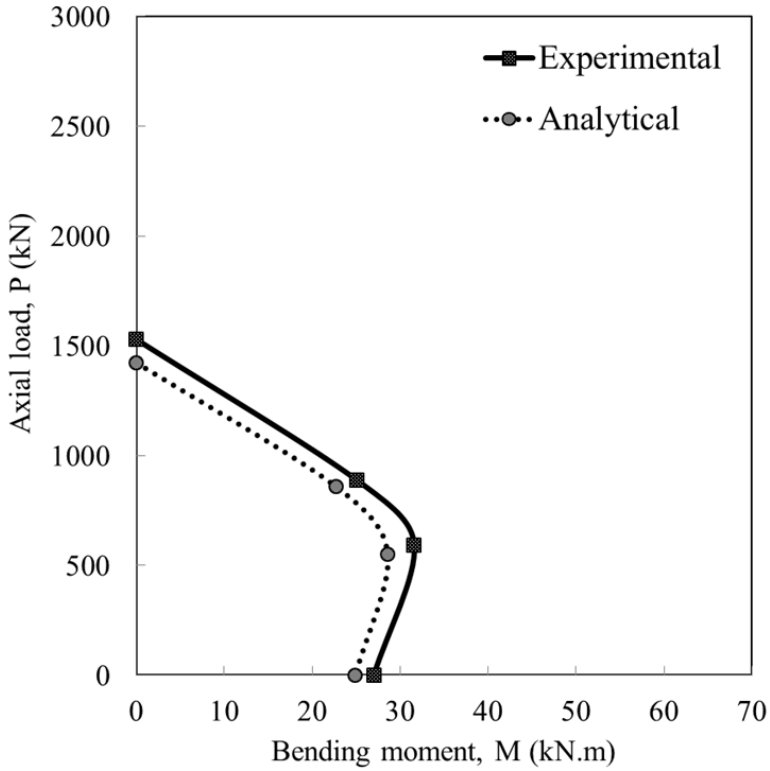

Fig. 5. Experimental and analytical axial load bending moment interactions of REF group

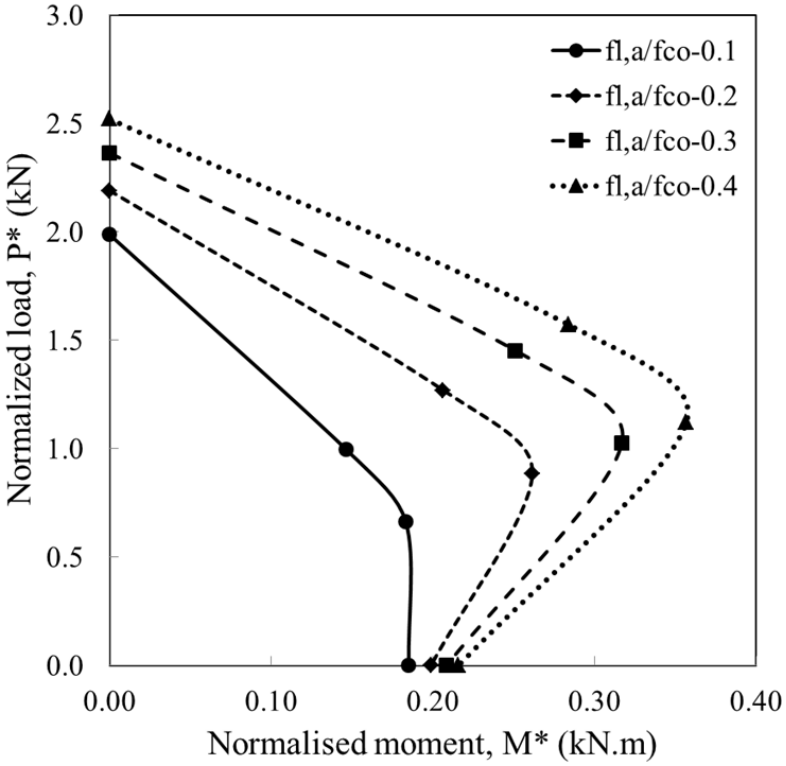

(a)

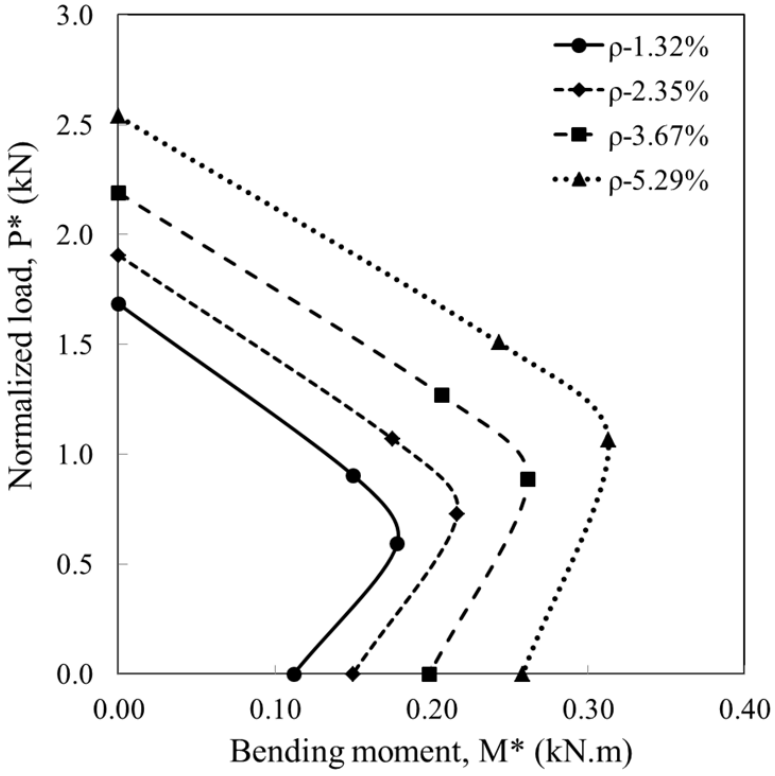

Fig. 6. Normalized

(b)

$P^* - M^*$ interactions of GTGR group for different (a) actual confinement ratios, and (b) reinforcement ratios